Design and growth of dendritic Cu$_{2-x}$Se and bunchy CuSe hierarchical crystalline aggregations†

Dapeng Li,[a] Zhi Zheng,*[a] Yan Lei,[a] Suxiang Ge,[ab] Yidong Zhang,[a] Yange Zhang,[a] Ka Wai Wong,[a] Fengling Yang[a] and Woon Ming Lau[c]

Dendritic nanocrystals of copper selenide were fabricated *in situ* for the first time by using alcohol as the solvent. Cu$_{2-x}$Se films composed of hierarchically ordered dendritic nanostructures were prepared on Cu substrates at a rather moderate temperature of 190–200 °C for just 1–3 h, while bunchy CuSe nanostructures could be further constructed above the Cu$_{2-x}$Se dendrites by prolonging the reaction time of solvothermal growth with ethanol as the solvent. The resulting Cu$_{2-x}$Se nanodendrites display highly symmetric corolitic morphology while the bunchy CuSe aggregations show particular nanostructures with a pronounced trunk and actinomorphic multi-branches. It is also found that the dendritic structures of crystalline Cu$_{2-x}$Se could never be obtained when the reaction temperature is less than 190 °C, while the temperature needed is 160 °C for Ag$_2$Se nanodendrites and higher than 220 °C for CdSe nanodendrites. These copper selenide nanostructures with hierarchically ordered 3-dimensional (3D) framework exhibited good absorbance and photoluminescence (PL) property and could bear potential applications in solar cell devices in the future.

1. Introduction

Dendritic nanocrystals are novel architectures generally assembled by various structural monomers. Earlier studies on the dendrite formation were mainly based on metal cast and jointing experiments.[1] Up to now, some nanoscale dendrites have been synthesized including pure metal and metal chalcogenide dendrites. For example, well-defined silver nanodendrites were synthesized by a replacement reaction between AgNO$_3$ and zinc plate in aqueous solution,[2] or *via* a mixing process of AgNO$_3$ aqueous solution through dropping into Zn microparticle suspension.[3] In our previous experiments, we have successfully presented a very simple reaction strategy for an *in situ* fabrication of highly oriented (001) nanocrystalline Ag$_2$Se dendrites.[4] Hierarchical cadmium sulfide (CdS) nanodendrites were also synthesized by a simple hydrothermal treatment with CdCl$_2$ and thiourea as Cd and S sources, respectively, and poly (ethylene glycol) (PEG) as a capping agent.[5] At the same time, Cho's group prepared hyperbranched CdS nanodendrites by introducing *N,N*-dimethylformamide (DMF) as a medium in the same CdCl$_2$ and thiourea reaction system.[6] Recently, copper sulfide dendrites have been prepared in high yield by a concentration-controlled reaction of ethylenediamine (EDA) and tributylphosphite

(TBPT).[7] Despite the fabrication of considerable metal selenides and sulfides with dendritic structures, to the best of our knowledge, copper selenide nanodendrites have not so far been reported.

Copper selenides are very important p-type semiconductors, which have potential applications in solar cells,[8] gas sensors,[9] super ionic conductors[10] and thermoelectric converters,[11] *etc.* As a kind of binary compound, copper selenide can exist in a wide range of stoichiometric compositions (CuSe, Cu$_2$Se, CuSe$_2$, Cu$_3$Se$_2$, Cu$_5$Se$_4$, Cu$_7$Se$_4$, *etc.*) and non-stoichiometric compositions (Cu$_{2-x}$Se),[12] and can be constructed into several crystallographic forms (monoclinic, cubic, tetragonal, hexagonal, *etc.*).[13] Especially, Cu$_{2-x}$Se was reported to possess a direct band gap of 2.2 eV and indirect band gap of 1.4 eV for $x = 0.2$,[14] which can offer a high efficiency of conversion. In the previous fabrication experiments of crystalline copper selenides, much effort has been focused on the depositions of copper selenide crystals on a special substrate by a solution growth technique. In a typical procedure of this technique, CuCl$_2$ (or CuSO$_4$) and a freshly prepared solution of Na$_2$SeSO$_3$ are usually used in alkaline media to deposit crystalline copper selenides on microscope glass substrates.[15,16] Particularly, several groups synthesized simple 0-dimensional and 1-dimensional copper selenide nanocrystals by some liquid chemical methods. For example, O'Brien first synthesized the tri-*n*-octylphosphine oxide (TOPO)-capped CuSe quantum dots *via* a single-source precursor Cu(Se$_2$CNEt$_2$)$_2$.[17] Zhang's group developed a novel method for crystalline nanotubes of CuSe, in which trigonal Se nanotubes were used as a template-directed reagent.[18] Recently, long crystalline Cu$_{2-x}$Se nanowire bundles with diameters of 100–300 nm and lengths up to hundreds of micrometres were synthesized in a large scale.[9] Very recently, Deng's group reported the synthesis of two-dimensional single-crystal

[a]Institute of Surface Micro and Nano Materials, Xuchang University, Xuchang, 461000, China. E-mail: zhengzhi9999@yahoo.com.cn; Fax: +86 374 4369209; Tel: +86 374 4369209
[b]Key Laboratory of Pesticide & Chemical Biology of Ministry of Education, College of Chemistry, Central China Normal University, Wuhan, 430079, China
[c]Surface Science Western, The University of Western Ontario, London, Canada
† Electronic supplementary information (ESI) available: SEM morphologies of dendritic CdSe nanocrystals. See DOI: 10.1039/b919087m

berzelianite ($Cu_{2-x}Se$) nanosheets and nanoplates.[19] Nevertheless, hierarchically ordered 3-dimensional (3D) nanodendrites of copper selenide have not yet been synthesized.
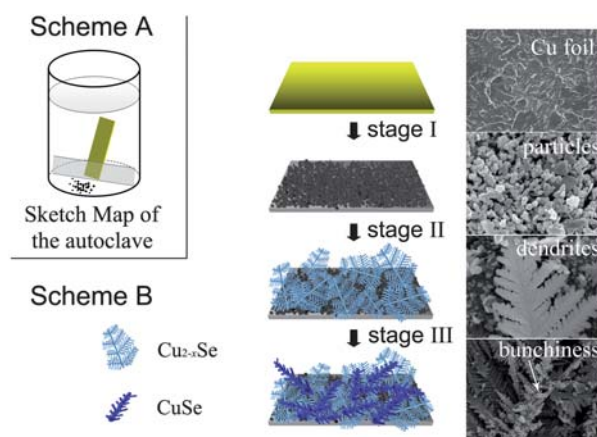
The importance of fabricating hierarchically ordered copper selenide nanostructures lies in that semiconducting copper selenides could show preponderant photoelectric functions which are derived from the advanced morphology. For some examples in solar cell devices, 2-dimensional or 3-dimensional (2D or 3D) nanostructures or nanowebs of crystalline semiconductors could show higher efficiency of PV conversion than the simple particles and 1-dimensional (1D) materials (nanorods or nanowires), since the 2D or 3D nanostructured semiconductors can effectively transport holes or electrons *via* the interconnected networks in the scaffolds.[20] Nanodendrites, which essentially possess much more advantages than nanosheets and nanoplates in solar cell applications, are indeed such network materials and their 3D dendritic nanostructures can provide both the electrical links and a high surface/volume ratio.

In this article, we describe a mild, template free and environmental friendly route to fabricate crystalline copper selenides which include hierarchically ordered dendritic $Cu_{2-x}Se$ and bunchy CuSe nanocrystals. We also investigated the evolution of these two copper selenide nanodendrites and found that the differences in stoichiometric compositions and crystal phase of them were mainly resulted from the release and diffusion effect of Cu cations towards Cu–Se reaction interface in the solvothermal reaction system saturated with selenium.

2. Experimental

All reagents were of analytical grade. In a typical procedure, a piece of copper foil (Tianjin Dengfeng Chemical Reagent Factory, China) was dipped in a diluted HCl solution under ultrasonic irradiation for 5 min to remove the copper oxide and other impurities on the copper foil. The purified copper foil, 0.010 g selenium powder (Sinopharm Chemical Reagent Co., Ltd), and 15 mL of 1-hexanol (or ethanol) were placed in a 20 mL tailor-made Teflon-lined autoclave. A piece of thin microscope glass (23 mm × 8 mm, $d = 1$ mm) was placed in the bottom of the autoclave (see Fig. 1, Scheme A) to separate Se powder from the Cu foil, so that as-prepared copper selenide nanocrystals can also be separated from the un-reacted Se powder. The autoclave was maintained at 190 °C for 1 h (or 3 h), and then cooled to room temperature. The copper foil and casts on the bottom of the autoclave were taken out of the solution and washed with ethanol followed by distilled water for several times. Finally the as-prepared copper selenide films on Cu foil was dried in air and the casts were dried at 80 C lasting 2 h for characterization.

All X-ray diffraction (XRD) patterns were recorded with a Philips MPD 18801 diffractometer using Cu Kα radiation. Morphological investigations were performed with a JSM-5600 scanning electron microscopy (SEM). The nanostructures and the selected area electron diffraction (SAED) patterns of the resulting copper selenide dendrites were recorded by a Philips CM-120 transmission electron microscopy (TEM). The samples for TEM were prepared by dispersing the precipitates in ethanol, and then the dispersion were dropped on carbon-copper grids. The X-ray photoelectron spectra (XPS) of the products were collected with a Kratos AXIS ULTRA instrument, with Mg Kα

Fig. 1 Sketch map of the autoclave (Scheme A); schematic diagram of the growth procedure of copper selenides (Scheme B). In Scheme B, stage I shows the initial selenizing process, which results in the formation of particles on the surface of copper foil in solvothermal system; stage II shows the formation of $Cu_{2-x}Se$ dendrites above the particles; stage III shows that the CuSe bunchy nanostructures formed above the $Cu_{2-x}Se$ dendrites. The four SEM pictures in the right of Scheme B shows the corresponding images of bare copper surface, copper selenide particles, $Cu_{2-x}Se$ dendrites, and CuSe bunchy nanostructures, respectively.

X-ray as the excitation source. UV-vis absorption spectra were obtained using a Perkin Elmer Lambda 35 UV-VIS Spectrometer equipped with a labsphere diffuse reflectance accessory. For photoluminescence (PL) spectroscopy, a Spex spectrofluorometer with a xenon lamp as excitation source was used.

3. Results and discussion

3.1 Formation and characterization of $Cu_{2-x}Se$ dendrites

We performed a manifold analysis of morphology and structure so as to get a detailed characterization of the as-prepared $Cu_{2-x}Se$ dendrites. Fig. 2 shows the SEM, TEM, HRTEM, SAED, and XRD results of the $Cu_{2-x}Se$ dendrites after solvothermal treatment at 190 °C for 3 h with 1-hexanol as the solvent. The morphology of the $Cu_{2-x}Se$ dendrites grown on the Cu foil surface is displayed in Fig. 2a and 2b. Dendritic $Cu_{2-x}Se$ nanocrystals with various dimensions can be obtained within a large area of Cu foil surface (Fig. 2a). The upper inset of Fig. 2a shows a magnified image of the dendritic $Cu_{2-x}Se$ nanocrystals from the rectangle area, while the nether inset shows the magnified copper selenide nanoparticles which maybe the initial products resulted from chemical adsorption between solvated selenium and Cu atom surface layer. A clear and perfect $Cu_{2-x}Se$ dendrite with hierarchically ordered secondary and tertiary branches (nanorods) is shown in Fig. 2b. It can be observed that the nanodendrite is highly symmetric, the lateral branches grow symmetrically on two sides of a central trunk and keep about 60 angles with respect to the central trunk. Both the trunk and the branches are about 50 nm in diameter. The growth mode of the tertiary branches is almost the same with that of the secondary ones.
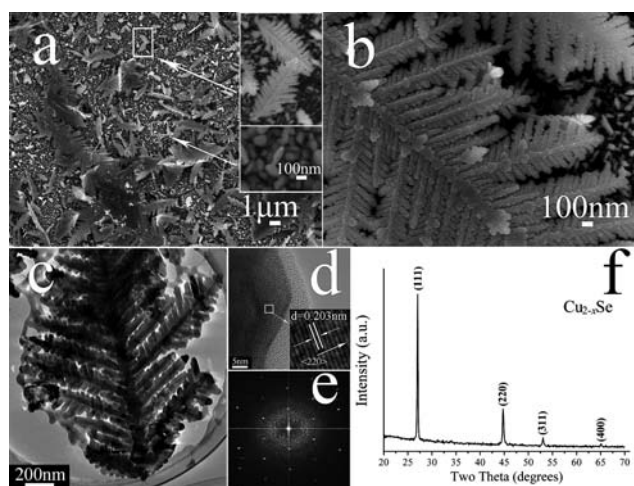
Fig. 2 Low-resolution SEM image (a) and high-resolution SEM image (b) of $Cu_{2-x}Se$ dendrites *in situ* grown on copper foil surface *via* a solvothermal reaction. The upper inset displays the magnified morphology of the rectangle area in (a) and the nether one shows the magnified morphology of the nanoparticles grown on the copper foil surface from the nether rectangle area in (a). The low-resolution TEM image obtained from one of these dendrites is given in (c). The high-resolution TEM image (d) was recorded from tip of one branch in a dendrite. Image (e) gives a selected area electron diffraction (SAED) pattern that was obtained by focusing the electron beam on a tip shown in image (d). The XRD pattern of $Cu_{2-x}Se$ dendrites is recorded in image (f).

The morphology and structure of the $Cu_{2-x}Se$ dendrites was further investigated by transmission election microscopy (TEM), high-resolution transmission election microscopy (HRTEM) and selected-area electron diffraction (SAED) pattern. Fig. 2c illustrates a TEM image of a typical $Cu_{2-x}Se$ dendritic nanostructure at a low magnification. The HRTEM image in Fig. 2d shows the region at a branch tip. The inset of Fig. 2d displays the clear lattice fringes. The fringe spacing is 0.203 nm, which is very close to the interplanar spacing of (220). The selected area electron diffraction (SAED) pattern from the branch tip in Fig. 2e confirms its single crystalline nature. In order to avoid contamination of un-reacted Se, we placed a small glass slice on the bottom of the autoclave (as shown in Fig. 1), so as to effectvely separate the un-reacted Se powder from the as-synthesized copper selenide crystals and control the diffusion of solvated Se towards Cu foil in the solvothermal system for controllable fabrication of pure copper selenide dendrites. Fig. 2f displays the corresponding XRD pattern of $Cu_{2-x}Se$ dendrites collected from the casts on the bottom of an autoclave to avoid the strong signals from the Cu foil. The four diffraction peaks can be indexed to the (111), (220), (311), and (400) diffraction of face-centered cubic (fcc) $Cu_{2-x}Se$ (JCPDS Card File, 6–680). All characterization results show that the products from the present solvothermal system of Cu foil and elemental selenium are pure $Cu_{2-x}Se$ nanodendrites.

The synthesis of copper selenides by general templating method may result in the oxidation of little Se in the product.[18] To confirm the purity of the resulting products, Fig. 3 shows the XPS survey, Cu 2p and Se 3d core level spectra of the $Cu_{2-x}Se$ dendrites/films obtained from Se/1-hexanol system for 3 h at 190 C with a selenium concentration of 7×10 g mL^{-1}
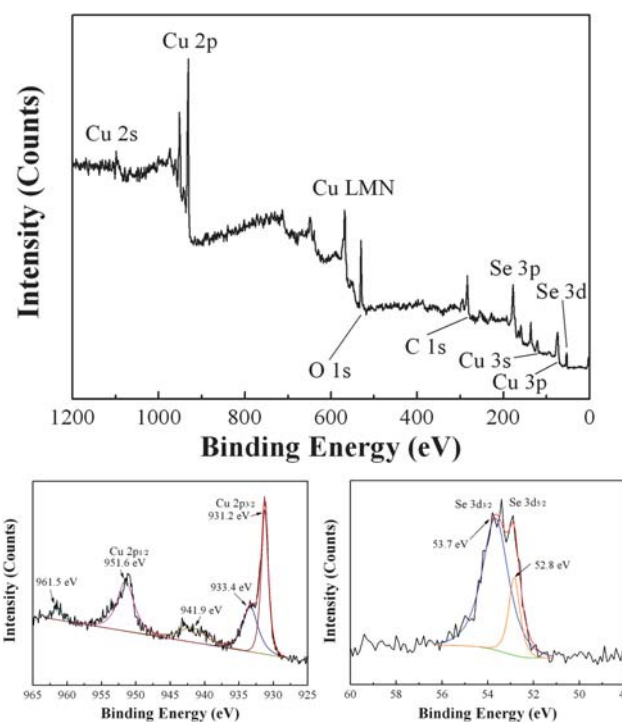

Fig. 3 XPS Cu 2p, Se 3d core level spectra and survey spectrum of $Cu_{2-x}Se$ dendrites/films generated from Se/1-hexanol system for 3 h at 190 °C with the selenium concentration of 6.67×10^{-4} g mL^{-1}.

(0.010g/15mL). The Cu 2p3/2, Cu 2p1/2, Se 3d5/2 and Se 3d 3/2 core levels appear at the binding energies of 931.2 eV, 951.6 eV, 52.8 eV, and 53.7 eV, respectively. No shoulder peaks originated from oxidized Se could be seen, which confirmed the formation of pure $Cu_{2-x}Se$ in the present solvothermal condition. The presence of small peaks of oxygen and carbon in XPS survey spectrum are originated from the contamination before XPS test.

3.2 Design and growth of bunchy CuSe nanocrystals by increasing reaction time

Considering that the further growth of $Cu_{2-x}Se$ dendrites on Cu foil will be decelerated by the obstructed effect of $Cu_{2-x}Se$ layer formed at the interface of Cu foil and solvated Se in the above reaction system, we designed a new experiment by employing the low-viscosity ethanol as solvent and set the reaction temperature at 200 °C to obtain better liquidity and accelerate the Cu–Se chemical reaction. More details on the dissolution behaviour of Se in solvothermal system can be found in the literature.[21]

Fig. 4a shows the SEM micrographs of dendritic crystals grown on Cu foil obtained at 200 °C for 1 h in ethanol with a Se concentration of 7×10 g mL^{-1}. Compared with the dendritic crystals synthesized in 1-hexanol solvothermal system, it is observed that the secondary and tertiary branches array in high density and have a tendency to form an integral flake-like structure in some branch tips. The corresponding XRD patterns of dendrites/film were recorded to reveal the quality of resulting copper selenide crystals/film (Fig. 4b). Because of the relatively high intensity of Cu substrate diffraction peaks, only diffraction peaks from (111), (220), and (311) of $Cu_{2-x}Se$ can be detected.
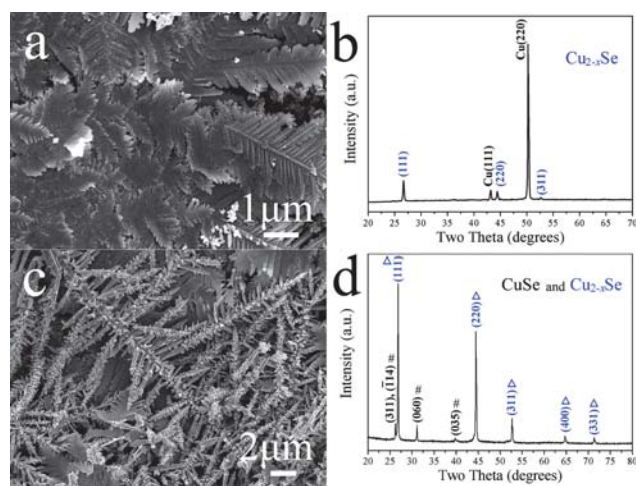
Fig. 4 SEM images of pure $Cu_{2-x}Se$ dendrites grown on Cu foil substrate (a). The corresponding XRD patterns of $Cu_{2-x}Se$ dendrites and the Cu substrate (b). SEM images of mixture of $Cu_{2-x}Se$ dendrites and CuSe bunchiness grown on Cu substrate (c). The corresponding XRD patterns (d) of the mixture of $Cu_{2-x}Se$ and CuSe nanocrystals. (#, CuSe; △, $Cu_{2-x}Se$).

When the reaction time was prolonged to 3 h in this solvothermal system, some unique nanostructures, *i.e.* a pronounced trunk with short actinomorphic multi-branches formed, which were denominated as bunchy structures in Fig. 4c. Interestingly, these bunchy structures distributed within large areas above the $Cu_{2-x}Se$ dendrites surface, indicating that the upper bunchy structures were initiated on the $Cu_{2-x}Se$ dendrites covered Cu foil by prolonging the solvothermal reaction time. The corresponding XRD patterns confirmed the formation of a new crystal phase apart from the firstly generated $Cu_{2-x}Se$ nanodendrites (Fig. 4d). These new diffraction peaks which include (311), ($\bar{1}$14), (060) and (035) can be well indexed with the monoclinic CuSe (JCPDS Card File, 49–1456). Since the nanodendrites layer has been identified as the $Cu_{2-x}Se$ phase, it can thus be deduced that the newly formed bunchy nanocrystals are resulted from the new CuSe crystal phase. After the formation of the first $Cu_{2-x}Se$ nanodendrites layer on the Cu foil, the pervasion of Cu cations from the Cu foil was restricted. The scarce of Cu cations at the reaction interface may facilitate the formation of 1 : 1 CuSe with less Cu component. Therefore, the formation of CuSe bunchy structures may mainly attribute to the limited dispersion of Cu cations towards Cu–Se reaction interface under non-equilibrium conditions.

3.3 Possible mechanisms for the growth of dendritic $Cu_{2-x}Se$ and bunchy CuSe

Before the crystal growth, there are two preliminary processes that are necessary, including the dissolution of the Se powder and transportation of the solvated Se to the Cu foil. Then, a schematic diagram was proposed to explain the growth process of the two different hierarchically ordered copper selenides as shown in Fig. 1. Scheme A (top left corner) shows the inside view of the autoclave in our experiments. A thin piece of microscope glass was so placed to separate the desquamative copper selenide from the un-reacted selenium powder. Cu foil was placed slantways

towards the inner wall of an autoclave. Scheme B illustrates the three stages (*i.e.*, stage I, stage II and stage III) of the growth of copper selenides on Cu foil surface. The real morphologies on the right display the SEM images corresponding to the left schematic maps at different stages. Stage I shows the initial selenizing process, in which the resulting copper selenide nanoparticles formed directly on the Cu foil surface. The crystalline copper selenide particles have an average size of less than 100 nm. Stage II demonstrates the well-defined $Cu_{2-x}Se$ dendrites assembled *via* the self-organization of adjacent nanoparticles. In this step, the formation of dendritic $Cu_{2-x}Se$ aggregations may attribute to the well-known "oriented attachment" mechanism.[22] It is noteworthy that the formation of dendritic $Cu_{2-x}Se$ nanocrystals at Stage II is similar to that of Ag_2Se[4] crystals reported in our previous research. Stage III demonstrates the further growth of bunchy CuSe nanostrucures above the surface of the dendritic $Cu_{2-x}Se$ aggregations. In this final stage, the gradually weakened penetration of limited Cu cations originated from Cu foil could result in the formation of the 1 : 1 CuSe bunchy structures in which the relative amount of Se became higher. Release efficiency of Cu cations is believed to be a key factor in determining the crystal structure and morphology of the products: planar dendritic $Cu_{2-x}Se$ or 3-dimensional bunchy CuSe.

3.4 The key role of reaction temperature in fabricating the dendritic structures of metal selenide nanocrystals.

A main purpose of our present work is to find an effective way to fabricate various metal selenides with hierarchically ordered dendritic structures. In the solvothermal process of preparing dendritic metal selenides, we found that the reaction temperature plays the key role in determining the final dendritic and bunchy morphologies of the resulting nanocrystals. For example, when the reaction temperature was set at less than 190 °C, the hierarchically ordered structures could never been obtained even if the reaction time was prolonged to 12 h for the synthesis of copper selenides (SEM picture not shown). Two parallel experiments for solvothermally fabricating copper selenide crystals at 160 °C and 220 °C were performed to investigate the influence of reaction temperature. Interestingly, the products prepared at 160 °C were only nanoparticles, while the products obtained at 220 °C displayed the same dendritic morphologies (SEM pictures not shown) with those prepared at 190 °C.

Differently in our previous experiment, we have shown that hierarchically ordered crystalline Ag_2Se dendrites can easily be prepared at 160 °C in the similar hydrothermal condition.[4] Fig. 5 displays the two different hierarchically ordered nanodendrites of both crystalline $Cu_{2-x}Se$ and Ag_2Se, which were obtained at 200 °C and 160 °C, respectively. Comparing these two morphologies of $Cu_{2-x}Se$ and Ag_2Se dendrites, it was observed that the $Cu_{2-x}Se$ dendrites consisted of a long central trunk, highly hierarchical secondary and tertiary branches, and the growth of $Cu_{2-x}Se$ branches (nanorods) showed more orderly symmetry than that of the Ag_2Se dendrites. Furthermore, the average diameter of $Cu_{2-x}Se$ branch is smaller than that of Ag_2Se dendrite as seen from the SEM images. This is possibly related to the differences in chemical reactivity of Cu and Ag foil in solvothermal environments. Furthermore, for another metal selenides, dendritic structures of CdSe nanocrystals could only be
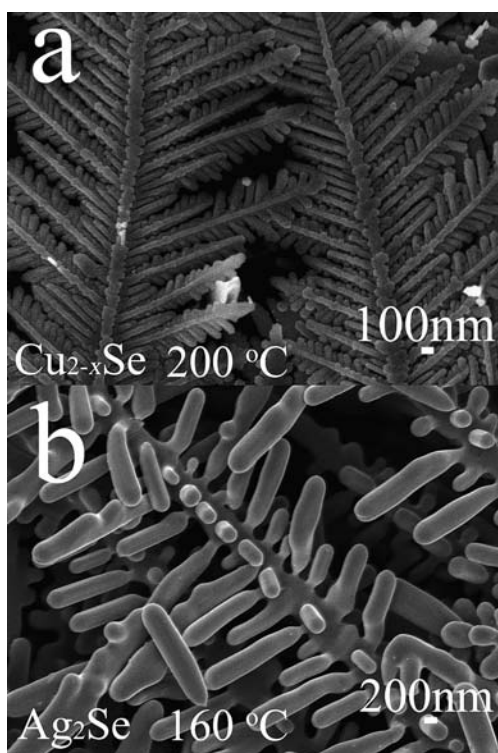
Fig. 5 SEM morphology of the $Cu_{2-x}Se$ dendrites prepared at 200 °C (a) and Ag_2Se dendrites prepared at 160 °C (b). The concentration of selenium in the ethanol-Se solvothermal system is fixed at 6.67×10^{-4} g mL^{-1}.

obtained when the reaction temperature was increased to 220 °C (see ESI).† Thus, we conclude that the reaction temperature is the key factor in determining the final dendritic structures of metal selenides in the solvothermal system.

3.5 The absorbability and photoluminescence of the synthesized $Cu_{2-x}Se$ dendrites/film

To characterize the optical performance of the dendritic $Cu_{2-x}Se$ nanocyrstals/film, we performed UV-vis absorption spectrum
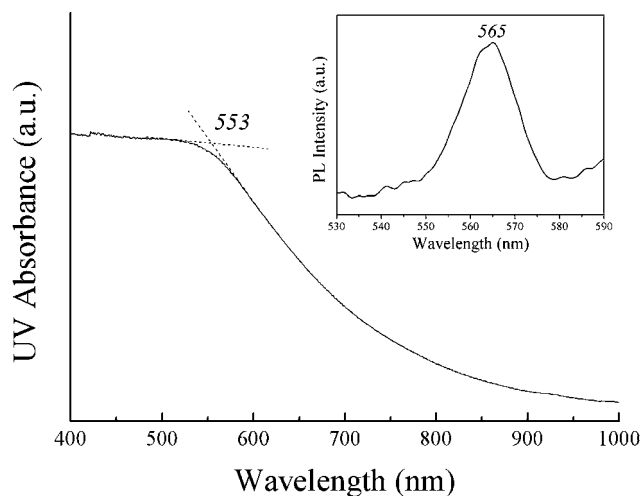

Fig. 6 UV-vis absorption spectra of the dendritic $Cu_{2-x}Se$ nanocrystals/film. The inset is the corresponding room-temperature PL emission spectra of the same dendritic products.

analysis. Fig. 6 depicts the UV-vis absorption spectrum of the corresponding $Cu_{2-x}Se$ dendrites obtained from the reported Se/1-hexanol solvothermal system. A broad absorption band was observed in the wavelength range of 400–700 nm. It was reported that $Cu_{2-x}Se$ with $x = 0.2$ possesses a direct band gap of 2.2 eV (absorption wavelength of 564 nm).[14] In the present experiment, the absorption edge observed at ∼553 nm that corresponds to a direct energy band gap of 2.24 eV is in good agreement with the reported value of non-stoichiometric $Cu_{2-x}Se$.[23] The photoluminescence (PL) spectrum was also recorded at room temperature. An emission band at ∼565 nm (2.20 eV) was observed as shown in the inset of Fig. 6. As compared to the result from the UV-visible spectrum, the emission band at 565 nm was assigned to the excitonic emission of $Cu_{2-x}Se$ *via* the radiative band-to-band recombination process.

4. Conclusions

In this paper, we describe the *in situ* fabrication of copper selenide films composed of two different hierarchically ordered dendritic $Cu_{2-x}Se$ and bunchy CuSe aggregations by a simple solvothermal reaction. The resulting $Cu_{2-x}Se$ nanodendrites display highly symmetric corolitic morphology while the bunchy CuSe aggregations show particular nanostructures with a pronounced trunk and actinomorphic multi-branches. Especially, the formation of CuSe bunchy structures may mainly attribute to the limited dispersion of Cu cations towards Cu–Se reaction interface under non-equilibrium conditions and release efficiency of Cu cations is believed to be a key factor in determining the crystal structure and morphology of the products: planar dendritic $Cu_{2-x}Se$ or 3-dimensional bunchy CuSe. More importantly, we found that the hierarchically ordered dendritic structures of crystalline $Cu_{2-x}Se$ could never be obtained when the reaction temperature is less than 190 °C, while the temperature needed is 160 °C for Ag_2Se nano-dendrites and higher than 220 °C for CdSe nanodendrites. The reaction temperature is the key factor in determining the final dendritic structures of metal selenides in the solvothermal system. Potentially, the methodologies reported here may provide a practical route for the development of dendritic nanostructures of other metal chalcogenide materials.

References

1 S. Henry, T. Minghetti and M. Rappaz, *Acta Mater.*, 1998, **46**, 6431.
2 J. X. Fang, H. J. You, P. Kong, Y. Yi, X. P. Song and B. J. Ding, *Cryst. Growth Des.*, 2007, **7**, 864.

3 X. G. Wen, Y. T. Xie, M. W. C. Mak, K. Y. Cheung, X. Y. Li, R. Renneberg and S. H. Yang, *Langmuir*, 2006, **22**, 4836.

4 D. P. Li, Z. Zheng, Z. Y. Shui, M. Q. Long, J. Yu, K. W. Wong, L. Yang, L. Z. Zhang and W. M. Lau, *J. Phys. Chem. C*, 2008, **112**, 2845.

5 Q. Q. Wang, G. Xu and G. R. Han, *Cryst. Growth Des.*, 2006, **6**, 1776.

6 M. H. Chen, Y. N. Kim, C. C. Li and S. O. Cho, *Cryst. Growth Des.*, 2008, **8**, 629.

7 W. P. Lim, H. Y. Low and W. S. Chin, *Cryst. Growth Des.*, 2007, **7**, 2429.

8 S. T. Lakshmikumar and A. C. Rastogi, *Sol. Energy Mater. Sol. Cells*, 1994, **32**, 7.

9 J. Xu, W. X. Zhang, Z. H. Yang, S. X. Ding, C. Y. Zeng, L. L. Chen, Q. Wang and S. H. Yang, *Adv. Funct. Mater.*, 2009, **19**, 1759.

10 C. Lévy-Clément, M. Neumann-Spallart, S. K. Haram and K. S. V. Santhanam, *Thin Solid Films*, 1997, **302**, 12.

11 V. M. Bhuse, P. P. Hankare, K. M. Garadkar and A. S. Khomane, *Mater. Chem. Phys.*, 2003, **80**, 82.

12 V. M. García, P. K. Nair and M. T. S. Nair, *J. Cryst. Growth*, 1999, **203**, 113.

13 R. D. Heyding and R. M. Murray, *Can. J. Chem.*, 1976, **54**, 841.

14 A. M. Hermann and L. Fabick, *J. Cryst. Growth*, 1983, **61**, 658.

15 S. R. Gosavi, N. G. Deshpande, Y. G. Gudage and R. Sharma, *J. Alloys Compd.*, 2008, **448**, 344.

16 B. Pejova and I. Grozdanov, *J. Solid State Chem.*, 2001, **158**, 49.

17 M. A. Malik, P. O'Brien and N. Revaprasadu, *Adv. Mater.*, 1999, **11**, 1441.

18 S. Y. Zhang, C. X. Fang, Y. P. Tian, K. R. Zhu, B. K. Jin, Y. H. Shen and J. X. Yang, *Cryst. Growth Des.*, 2006, **6**, 2809.

19 Z. T. Deng, M. Mansuripur and A. J. Muscat, *J. Mater. Chem.*, 2009, **19**, 6201.

20 I. Gur, N. A. Fromer, C. P. Chen, A. G. Kanaras and A. P. Alivisatos, *Nano Lett.*, 2007, **7**, 409.

21 J. Lu, Y. Xie, F. Xu and L. Y. Zhu, *J. Mater. Chem.*, 2002, **12**, 2755.

22 Y. Cheng, Y. S. Wang, D. Q. Chen and F. Bao, *J. Phys. Chem. B*, 2005, **109**, 794.

23 Y. J. Hsu, C. M. Hung, Y. F. Lin, B. J. Liaw, T. S. Lobana, S. Y. Lu and C. W. Liu, *Chem. Mater.*, 2006, **18**, 3323.